

Comprehensive modeling study of ozonolysis of oleic acid aerosol based on real-time, online measurements of aerosol composition

Gallimore, P. J.; Griffiths, P. T.; Pope, F. D.; Reid, J. P.; Kalberer, M.

DOI:

[10.1002/2016JD026221](https://doi.org/10.1002/2016JD026221)

License:

None: All rights reserved

Document Version

Peer reviewed version

Citation for published version (Harvard):

Gallimore, PJ, Griffiths, PT, Pope, FD, Reid, JP & Kalberer, M 2017, 'Comprehensive modeling study of ozonolysis of oleic acid aerosol based on real-time, online measurements of aerosol composition', *Journal of Geophysical Research: Atmospheres*. <https://doi.org/10.1002/2016JD026221>

[Link to publication on Research at Birmingham portal](#)

Publisher Rights Statement:

Copyright 2017. American Geophysical Union. All Rights Reserved.

General rights

Unless a licence is specified above, all rights (including copyright and moral rights) in this document are retained by the authors and/or the copyright holders. The express permission of the copyright holder must be obtained for any use of this material other than for purposes permitted by law.

- Users may freely distribute the URL that is used to identify this publication.
- Users may download and/or print one copy of the publication from the University of Birmingham research portal for the purpose of private study or non-commercial research.
- User may use extracts from the document in line with the concept of 'fair dealing' under the Copyright, Designs and Patents Act 1988 (?)
- Users may not further distribute the material nor use it for the purposes of commercial gain.

Where a licence is displayed above, please note the terms and conditions of the licence govern your use of this document.

When citing, please reference the published version.

Take down policy

While the University of Birmingham exercises care and attention in making items available there are rare occasions when an item has been uploaded in error or has been deemed to be commercially or otherwise sensitive.

If you believe that this is the case for this document, please contact UBIRA@lists.bham.ac.uk providing details and we will remove access to the work immediately and investigate.

1 **Comprehensive modelling study of ozonolysis of oleic acid aerosol based on real-time,**
2 **online measurements of aerosol composition**

3 **P.J. Gallimore¹, P.T. Griffiths¹, F.D. Pope², J.P. Reid³ and M. Kalberer¹**

4 ¹Department of Chemistry, University of Cambridge, Lensfield Road, Cambridge, CB2 1EW,
5 UK.

6 ²School of Geography, Earth and Environmental Sciences, University of Birmingham,
7 Edgbaston, Birmingham, B15 2TT, UK.

8 ³School of Chemistry, University of Bristol, Bristol, BS8 1TS, UK.

9
10 Corresponding authors: Peter Gallimore (pjpg48@cam.ac.uk), Paul Griffiths (ptg21@cam.ac.uk)

11
12 **Key Points:**

- 13 • Extractive Electrospray Ionisation Mass Spectrometry can be used to assess reaction
14 kinetics in oleic acid aerosols.
- 15 • The most important sinks for Criegee intermediates formed during oleic acid ozonolysis
16 are isomerization and secondary ozonide formation.
- 17 • The Pretty Good Aerosol Model can reproduce measurements of evolving reactant loss,
18 product formation and particle size change.
19

20 Abstract

21 The chemical composition of organic aerosols profoundly influences their atmospheric
22 properties, but a detailed understanding of heterogeneous and in-particle reactivity is lacking. We
23 present here a combined experimental and modelling study of the ozonolysis of oleic acid
24 particles. An online mass spectrometry (MS) method, Extractive Electrospray Ionization (EESI),
25 is used to follow the composition of the aerosol at a molecular level in real time; relative changes
26 in the concentrations of both reactants and products are determined during aerosol aging. The
27 results show evidence for multiple non first order reactions involving stabilized Criegee
28 intermediates, including the formation of secondary ozonides and other oligomers. Offline
29 Liquid Chromatography (LC) MS is used to confirm the online MS assignment of the
30 monomeric and dimeric products. We explain the observed EESI-MS chemical composition
31 changes, and chemical and physical data from previous studies, using a process-based aerosol
32 chemistry simulation, the Pretty Good Aerosol Model (PG-AM). In particular, we extend
33 previous studies of reactant loss by demonstrating success in reproducing the time dependence of
34 product formation and the evolving particle size. This advance requires a comprehensive
35 chemical scheme coupled to the partitioning of semivolatile products; relevant reaction and
36 evaporation parameters have been refined using our new measurements in combination with PG-
37 AM.

38 **1. Introduction**

39 Organic compounds comprise a significant fraction of fine aerosol particle mass in the
40 atmosphere [Murphy *et al.*, 2006]. The chemical composition of both directly emitted, primary
41 organic particles and those formed by secondary processes is transformed continuously in the
42 atmosphere [Ziemann and Atkinson, 2012], with contingent but poorly understood influences on
43 the Earth's climate [Boucher *et al.*, 2013] and human health [Pope *et al.*, 2009].

44 Heterogeneous and in-particle reactions of organic compounds are particularly poorly
45 understood. In-particle reactivity is complicated by the strong influence of composition (aerosol
46 water content, ionic strength, organic functional group concentrations etc.) on observed reactions
47 and products [Kroll and Seinfeld, 2008]. In addition, identifying individual reaction pathways in
48 chemically complex mixtures is a difficult analytical and conceptual challenge [Noziere *et al.*,

49 2015]. Previous studies have attempted to quantify reactive uptake to particles [*Liggio and Li,*
50 2006; *Rudich et al., 2007*] and lifetimes of marker compounds in aerosols with respect to
51 heterogeneous oxidation [*Robinson et al., 2007; Zhao et al., 2014*]. The thermodynamic viability
52 of some reversible accretion reactions in particles have also been assessed [*Barsanti and*
53 *Pankow, 2005, 2006*]. In general, however, there is a need for detailed studies which elucidate
54 the major products, channels and pathways of in-particle reactions as a starting point for
55 assessing their atmospheric implications.

56 This study presents a combined measurement and modelling approach to understand product
57 formation mechanisms and kinetics during the heterogeneous ozonolysis of oleic acid (OA)
58 particles. Oleic acid is a low vapor pressure unsaturated fatty acid. Fatty acids are an important
59 class of compounds in the atmosphere [*Rogge et al., 1993; Mochida et al., 2002; Wang et al.,*
60 2006] and moreover OA aerosols have become an important test case for our understanding of
61 heterogeneous and in-particle reactions [*Ziemann, 2005; Zahardis and Petrucci, 2007*]. Here,
62 time-resolved molecular composition measurements are obtained from a recently developed
63 mass spectrometry (MS) technique, Extractive Electrospray Ionization (EESI) [*Gallimore and*
64 *Kalberer, 2013*]. EESI-MS is an online method capable of extracting and ionizing organic
65 analytes from aerosols to produce molecular ions with minimal fragmentation. Intensity changes
66 of reactant and product ions can be related to concentration changes in particles.

67 A few explicit or near-explicit models of organic aerosol chemistry have been described in recent
68 years [*Griffiths et al., 2009; McNeill et al., 2012; Berkemeier et al., 2013; Houle et al., 2015*].
69 These provide a flexible and rigorous framework in which to test our understanding of aerosol
70 chemistry and transport phenomena, in so far as relevant physico-chemical data are available.
71 Comparison with detailed measurements is essential for model validation; their predictive ability
72 can then be used to probe experimentally inaccessible phenomena, refine uncertain parameters
73 and provide a link between experiment and larger-scale models. Here, we use the Pretty Good
74 Aerosol Model (PG-AM) adapted from *Griffiths et al. [2009]*. Reaction, diffusion and interfacial
75 transport are represented explicitly in the model based on evaluated physical parameters derived
76 from the literature. We compare to a range of previous observations of oleic acid loss and
77 particle size change. We have also built a detailed chemical mechanism to capture the time

78 dependence of multi-generational product formation observed by EESI-MS, in particular
79 elucidate the fates of Criegee intermediates (CIs) formed during ozonolysis.

80

81 **2. Methods**

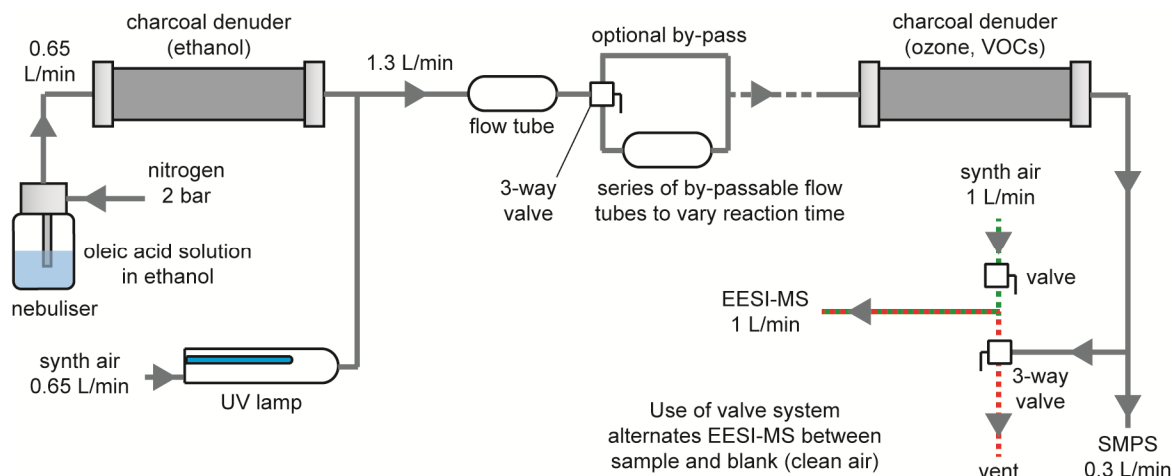
82 **2.1. Aerosol Flow Tube experiments**

83 Oleic acid particles were generated in the laboratory and reacted with ozone according to the
84 scheme in Figure 1. A solution of 3 mmol/L oleic acid (99%, Sigma Aldrich) in ethanol
85 (analytical reagent grade, Fisher) was prepared for use in a custom built constant-output
86 nebuliser. The nebuliser was supplied with nitrogen (oxygen-free, BOC) at a pressure of 2 bar
87 and output flow rate of 0.65 L/min. A charcoal denuder was employed to remove ethanol from
88 the particles, although small amounts (we estimate a few percent on a molar basis) were detected
89 in the MS analysis. No water was added to the system and the measured relative humidity (RH)
90 was less than 5% throughout the experiments. Ozone was produced by flowing synthetic air
91 (zero grade, BOC) through a photolysis tube containing a mercury UV lamp (Pen-Ray 3SC-9,
92 UVP) at 0.65 L/min. The concentration of ozone was varied by partially covering the lamp with
93 an aluminum sheath. It was varied between 8 and 22 ppm, determined after mixing with the
94 aerosol flow using a UV photometric ozone analyser (Thermo Scientific model 49i).
95 Experiments were performed in an air-conditioned laboratory at 20 °C.

96 A series of steady-state reaction times between oleic acid particles and ozone were established
97 using five by-passable flow tubes. The aerosol and ozone were mixed into a 4 mm inner diameter
98 PTFE tube. The Reynolds number (Re) of the fluid flow was calculated as $Re \sim 110$ and a
99 laminar mixing time < 0.1 s was therefore estimated based on *Keyser* [1984]. The reaction time
100 was estimated by dividing the total reaction volume by the volumetric flow rate. The total
101 reaction volume could be varied between 0.1-5.4 L resulting in reaction times of ~ 3 -140 s. A
102 second charcoal denuder was employed after the reaction volumes to remove any remaining
103 ozone and gas-phase organic species. The polydisperse aerosol size distribution was monitored
104 using a scanning mobility particle sizer (TSI model 3936). A single mode was observed with a
105 geometric standard deviation of 1.8, and a typical particle mass loading of 5 mg/m^3 . To account

106 for the full aerosol volume and surface area distributions, an “effective” average particle radius,
 107 $r_{\text{eff}} = 3V_t/S_t$, was calculated [Stewart *et al.*, 2004]. For fresh particles, r_{eff} was determined to be
 108 250 nm and was used as the particle radius in the model simulations described below.

109



110

111 Figure 1: Schematic diagram of laboratory setup for ozonolysis of oleic acid aerosol and chemical
 112 characterization. The ozone and aerosol were rapidly mixed so the exposure time was defined by the
 113 variable reaction volume between mixing and the second denuder. The steady state aerosol composition
 114 for a particular ozone exposure was acquired using EESI-MS, and the ion source was flushed with clean
 115 air between samples and “blank” spectra were recorded during this time.

116

117 2.2. EESI-MS operation

118 The EESI source is described in detail by Gallimore and Kalberer [2013]. Briefly, it consists of a
 119 custom-built aerosol injector and housing which is interfaced with a commercially-available
 120 electrospray ionisation (ESI) source (Thermo Scientific HESI-II). The primary solvent
 121 electrospray was a water-methanol 1:1 mixture (Optima LC-MS grade solvents, Fisher
 122 Scientific) containing 0.05% formic acid (90%, Breckland Scientific) and was operated in
 123 negative ionisation mode with a spray voltage of -3.0 kV. The aerosol injector delivered
 124 particles at a flow rate of 1 L/min into the primary solvent spray. Particle-droplet collisions
 125 dissolve the aerosol analytes, which are ionised and ejected into the gas phase by a Coloumb
 126 explosion mechanism typical for electrospray ionisation.

127 The EESI-MS acquisition was varied between blank and sample measurements from the aerosol
128 flow tube setup. Prior to blank measurements, air was flushed through the source for 15 minutes
129 to remove particles from the previous sample while the aerosol flow was diverted to a vent.
130 During sample measurements, the flushing air flow was switched off and the aerosol diverted
131 into the EESI source. This assured a constant flow of 1 L/min into the source was maintained at
132 all times. Mass spectrometry measurements were made using an ultra-high resolution mass
133 spectrometer (Thermo Scientific LTQ Orbitrap Velos). The high mass accuracy (<2 ppm) and
134 resolution ($m/\Delta m = 100\,000$ at m/z 400) of this instrument means that unambiguous molecular
135 formula assignments for reaction product ions are usually achieved.

136 Measurements were repeated three times for each reaction time and the standard deviation of the
137 relative peak intensities in the mass spectra were calculated (uncertainty on the ordinate in
138 kinetic plots). The largest uncertainty related to ozone exposure (abscissa in kinetic plots) was
139 the observation of limited quantities of oleic acid oxidation products (5-7 %) even before
140 deliberate ozone exposure. This prior exposure (for example in the nebulizer or during sample
141 preparation) was estimated by extrapolating best fit curves of the major products (azaleic acid
142 (AA), 9-oxononanoic acid (9-ON) and nonanoic acid (NA)) back to a hypothetical “zero”
143 intensity where they intercepted the ozone exposure axis. A prior exposure of 1.6×10^{-5} atm s
144 was estimated and used in Figures 4 and 5.

145 **2.3. Numerical Simulation of aerosol processes**

146 In support of the measurements, we compared the results against a numerical model of reactive
147 uptake of ozone by oleic acid aerosol. The Pretty Good Aerosol Model (PG-AM) describes the
148 coupled uptake from and evaporation to the gas phase, as well as coupled reaction/diffusion
149 processes occurring within the aerosol.

150 The approach is based on the work by *Griffiths et al.*, [2009] used in the study of reactive uptake
151 of N_2O_5 , in which the aerosol particle is treated as a series of concentric equal-volume shells, and
152 uptake is modelled as a series of coupled reaction-diffusion equations. For this work, diffusion
153 is parameterized as in *Griffiths et al.*, [2009] and the reactions treated by the coupled equations
154 were modified to include a mechanism for oleic acid ozonolysis including higher-order reactions
155 between products, as described in section 2.4. The model is based as far as possible on a

156 physically-based description of the chemistry and transport, and uses as input experimentally
157 accessible parameters such as diffusion coefficients and solubilities. Table S1 gives the
158 parameters employed here.

159 The model is written in Mathematica v10 (Wolfram) and the equations integrated forward in
160 time using the NDSolve routine. For this work, uptake to a single representative aerosol particle
161 was studied. The radius was set to the effective radius of the measured aerosol distribution ($r_{\text{eff}} =$
162 $3V_t/S_t$), and the time-dependence of aerosol components simulated for an initial pure oleic acid
163 particle on exposure to the measured ozone field. When comparing with our experiments, a
164 degree of uncertainty may be introduced by size-dependent uptake from a polydisperse aerosol
165 ensemble.

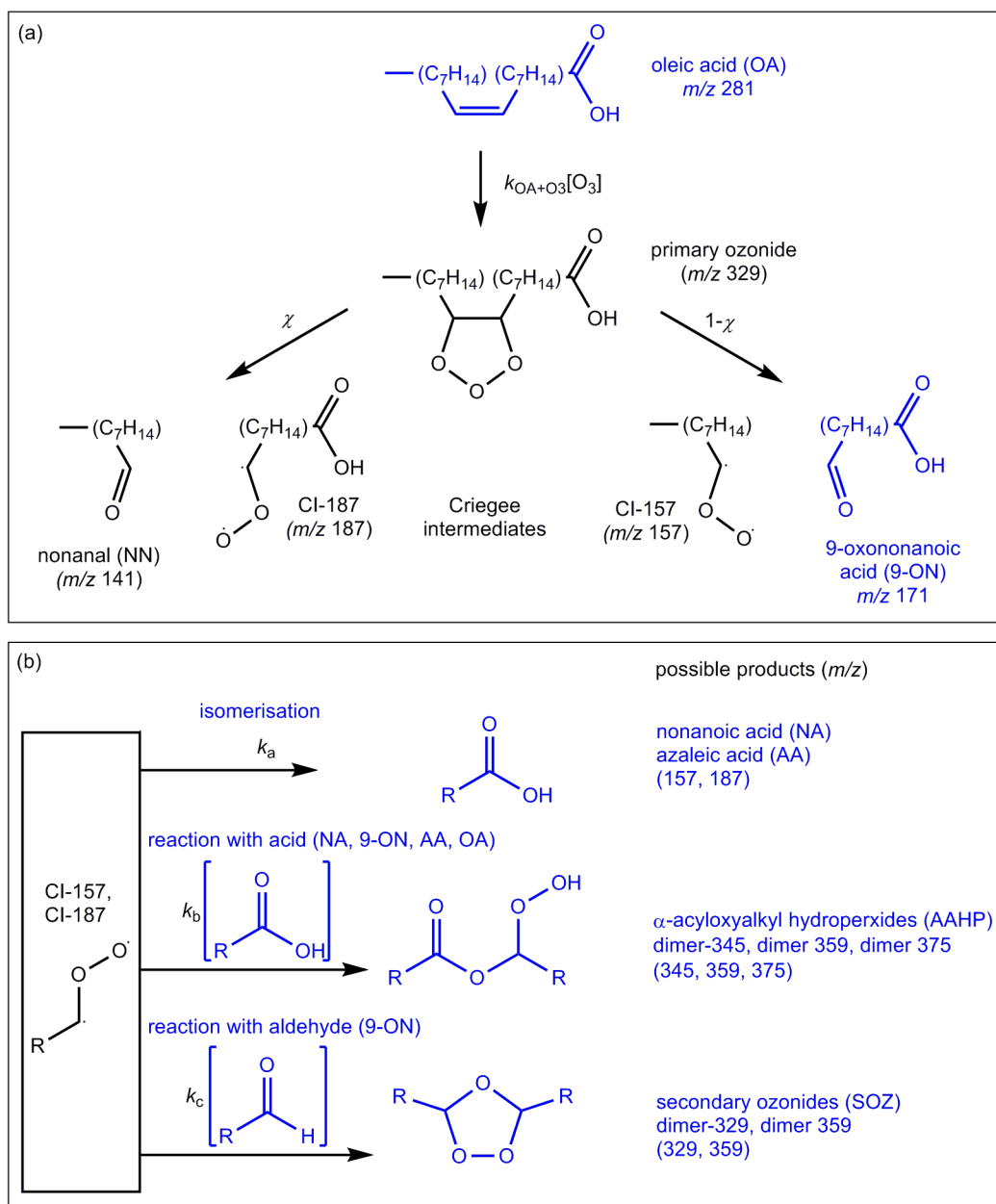
166 **2.4. Model mechanism for ozonolysis of oleic acid aerosol**

167 The formation of low molecular weight C₉ products from oleic acid ozonolysis has been
168 reviewed in the literature [Ziemann, 2005; Zahardis and Petrucci, 2007; Lee et al., 2012] and is
169 outlined in Figure 2(a). The ozone-alkene cycloaddition produces a short-lived primary ozonide
170 (POZ) which decomposes into an aldehyde and a rapidly stabilised Criegee intermediate (CI).
171 We assume CIs are stabilised in the subsequent discussion. Large nonanal (NN) yields have been
172 observed in previous studies [Vesna et al., 2009; Wang et al., 2016] suggesting that the NN + CI-
173 187 route is favored over the 9-oxononanoic acid (9-ON) + CI-157 route. Formation of nonanoic
174 and azaleic acids (NA, AA) from CIs is often described as a pseudo-unimolecular isomerization
175 [Ziemann, 2005] (k_a in Figure 2(b)) with a plausible mechanism proposed by Zahardis et al.,
176 [2005]. The model parameters $k_{\text{OA}+\text{O}_3}$, χ and k_a were estimated from the literature and are
177 detailed in Table S1.

178 The products formed from secondary reactions depend critically on the fates of the CIs. A
179 particular focus of our work is to better constrain the relative rates of these CI reactions.
180 Although a large number of reactions have been proposed in the literature, many of the proposed
181 mechanisms are speculative and the kinetics essentially unknown. We proceeded by introducing
182 simplifications to reduce parametric uncertainty in the model and align our mechanism with the
183 main dimeric products observed in our EESI-MS and LC-MS analysis (Figure 2(b)), and
184 previous studies [Zahardis et al., 2005; Reynolds et al., 2006; Lee et al., 2012]. This assigned a

185 single rate constant to all CI + carboxylic acid (k_b) and CI + aldehyde (k_c) reactions. Other
186 reactions were omitted altogether. CI self-reactions, second order in [CI], were neglected due to
187 the short CI lifetime and hence low steady state [CI]. The kinetics of CI + alkene reactions have
188 not been studied experimentally but the theoretical study of *Vereecken et al.*, [2014] concluded
189 that they are orders of magnitude slower than reactions with carboxylic acids and carbonyls for a
190 given CI. However, we note the very recent study of *Wang et al.*, [2016] and the earlier work of
191 *Katrib et al.*, [2004] which point to a potentially significant role for this reaction.

192 Omission of these potential CI sinks in the model may have led to overestimation of [CI] and
193 hence underestimation of k_b and k_c which were varied to obtain a good fit to the measured data in
194 the model. In addition, the missing CI + alkene reaction possibly underestimates the oleic acid
195 loss rate. However, this simplified mechanism minimizes the parametric uncertainty associated
196 with tuning the model rate constants to match the observations given the limited number of
197 assigned products. We also believe that it is chemically sensible to lump the rate constants based
198 on functional group reactivity.



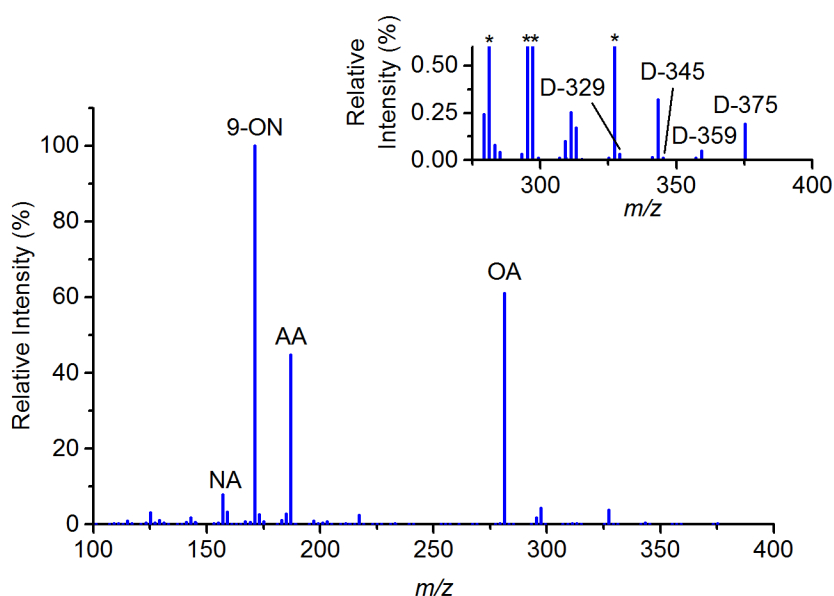
199

200 Figure 2: Chemical mechanism of oleic acid ozonolysis implemented in the model. (a) Primary C_9
 201 products and Criegee intermediates formed from the initial ozone-alkene cycloaddition. (b) Reactions of
 202 the Criegee intermediates: isomerisation to form carboxylic acids (k_a) and reactions with other functional
 203 groups to form dimers (k_b and k_c). k_{OA+O_3} , χ and k_a were estimated from the literature, k_b and k_c were
 204 adjusted to achieve the best fit to the measurements. We assign structures in blue to observed m/z , but
 205 assume the proposed black structures (intermediates and volatile products) would not be observed.

206 3. Experimental results and discussion

207 3.1. Product determination by mass spectrometry

208 A typical mass spectrum obtained from the EESI-MS analysis of oleic acid aerosol, partially
 209 oxidized with ozone, is given in Figure 3. The spectrum was acquired in negative ionization
 210 mode, meaning that functional groups which are readily deprotonated, such as carboxylic acids,
 211 are efficiently detected. Unreacted oleic acid was detected at m/z 281.2486. The peaks at m/z
 212 157.1234, 171.1027 and 187.0976 were assigned as the three low volatility C_9 products from
 213 Figure 2: nonanoic acid (NA), 9-oxononanoic acid (9-ON) and azaleic acid (AA). The other C_9
 214 product, nonanal (NN), is highly volatile and has been seen to partition into the gas phase [*Vesna*
 215 *et al.*, 2009] causing evaporative size changes [*Dennis-Smith et al.*, 2012]. In addition, its
 216 aldehyde functional group would not be readily ionized by deprotonation.



217

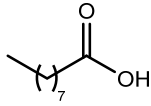
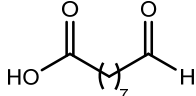
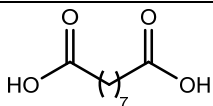
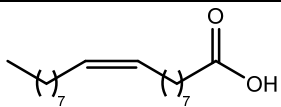
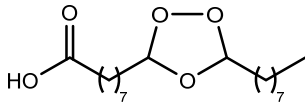
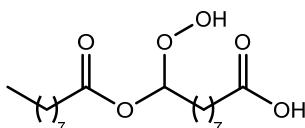
218 Figure 3: Mass spectrum of partially oxidized oleic acid aerosol acquired using EESI-MS. The initial
 219 particle-phase products of oleic acid ozonolysis, nonanoic acid (NA), 9-oxononanoic acid (9-ON) and
 220 azaleic acid (AA) are detected along with unreacted oleic acid (OA). The inset graph is an expansion of
 221 the region above m/z 275 which includes assignments of dimer products resulting from the reaction of
 222 primary products with Criegee intermediates. m/z intensities will be a function of both analyte
 223 concentration and ionization efficiency; we relate relative intensity changes to relative concentration
 224 changes in the aerosol, but note that the most intense peaks are not necessarily the most abundant aerosol
 225 species. The peaks marked (*) are cut off on the expanded scale.

226

227 The Criegee intermediates CI-157 and CI-187 are isobaric with NA and AA but we assume that,
 228 if detected, they do not make a significant contribution to the observed peak intensities due to
 229 their low concentrations. There is a small additional “monomer” peak at m/z 203.0925, also

230 observed by *Reynolds et al.*, [2006] which increases in intensity with ozone exposure and has a
 231 molecular formula consistent with a hydroperoxide product. This could form following
 232 decomposition of higher molecular weight products or reaction of the CIs with trace amounts of
 233 water. Other peaks in this region were not assigned and may be fragments or impurities from the
 234 electrospray solvent.

235 High molecular weight products are shown in the inset spectrum in Figure 3. The molecular
 236 formulae of the ions labelled “D” are consistent with dimers formed via CI-monomer reactions.
 237 Such products have been proposed in the literature and observed in previous studies [*Zahardis et*
 238 *al.*, 2005; *Reynolds et al.*, 2006; *Lee et al.*, 2012]. Our mechanism includes formation of these
 239 products as given in Figure 2(b). Specific possible structures for these species are given in Table
 240 S2. While the very recent study of *Wang et al.*, [2016] proposes a route to high molecular weight
 241 products via CI + alkene reactions, the proposed C₂₇ products were not identified in our
 242 measurements. The ions discussed here are listed in Table 1 for reference, along with potential
 243 structures and formation reactions.

<i>m/z</i>	Name and abbreviation	Possible structures (neutral)	Formation reaction
157.1027	Nonanoic acid (NA)		CI-157 isomerisation (<i>k_a</i>)
171.1027	9-Oxononanoic acid (9-ON)		OA + O ₃ (<i>k_{OA+O3}</i>)
187.0976	Azaleic acid (AA)		CI-187 isomerisation (<i>k_a</i>)
281.2486	Oleic acid (OA)		
329.2334	Dimer-329 (D-329)		9-ON + CI-157 (<i>k_c</i>) Secondary ozonide (SOZ)
345.2283	Dimer-345 (D-345)		NA + CI-187 (<i>k_b</i>) Hydroperoxide (α -AAHP)

			AA + CI-157 (k_c) Hydroperoxide (α -AAHP)
359.2075	Dimer-359 (D-359)		9-ON + CI-187 (k_c) Secondary ozonide (SOZ)
			9-ON + CI-187 (k_b) Hydroperoxide (α -AAHP)
375.2024	Dimer-375 (D-375)		AA + CI-187 (k_c) Hydroperoxide (α -AAHP)

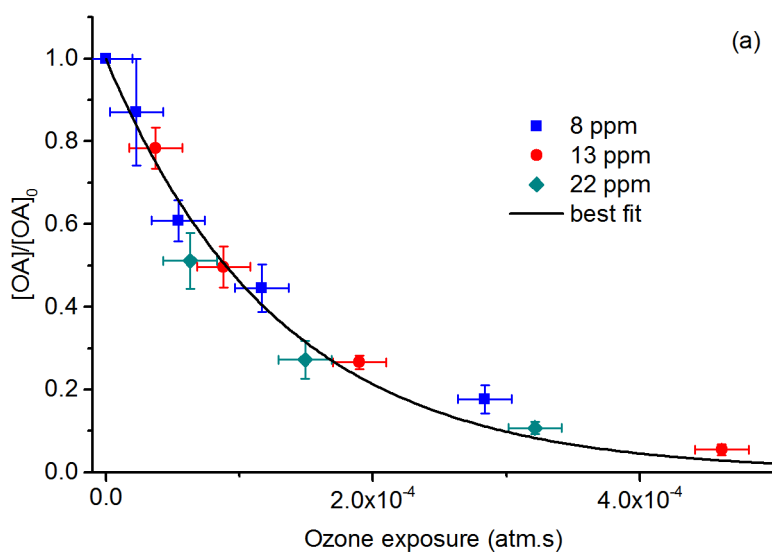
244 Table 1: Species detected via mass spectrometry in Figure 3 and Figure S1 which are products of
 245 ozonolysis considered in the model. Possible structures and the relevant formation reactions from Figure
 246 2 are also listed.
 247

248 Since LC-MS analysis involves separation and ionization of individual species according to
 249 retention time, it can be used to confirm that ions detected in direct infusion techniques
 250 correspond to stable molecular structures. LC-MS was applied here to oxidized oleic acid aerosol
 251 collected offline (described in the Supplementary Information, Figure S1). Distinct LC-MS
 252 peaks were identified for m/z 375.2024 and m/z 359.2075. The time dependence of these dimer
 253 ions in EESI-MS were therefore compared to the model calculations alongside the monomers.
 254 Corresponding chemistry for D-329 and D-345 was also included in the model but distinct LC-
 255 MS peaks could not be identified. Given the low abundance of these peaks in direct EESI-MS, it
 256 may be that they are lost in the LC-MS baseline, or are not as stable during aerosol collection,
 257 storage and extraction. The measured time dependence of m/z 329.2334 and 345.2283 was
 258 therefore not used to constrain the model performance.

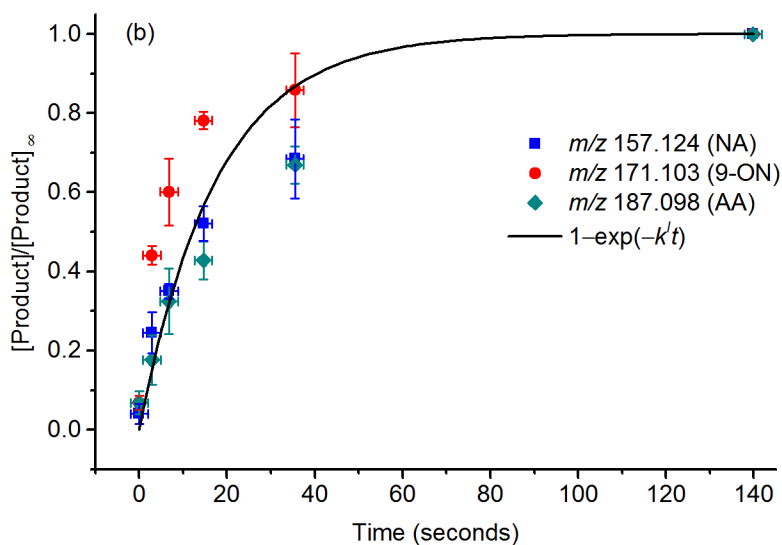
259 3.2. Kinetics of oleic acid loss

260 The kinetics of the heterogeneous reaction between oleic acid particles and ozone were
 261 monitored using EESI-MS. Relative particle-phase concentration changes were determined from
 262 relative intensity changes of reactant and product ions in the MS. The validity of this approach
 263 was demonstrated in *Gallimore and Kalberer* [2013] and is extended here to an ensemble of

264 particles whose composition is changing as a function of time. Figure 4(a) shows the intensity of
265 m/z 281.2486, assigned to deprotonated oleic acid $[\text{OA} - \text{H}]^-$, as a function of ozone exposure in
266 the flow tube. The OA signal intensity is scaled relative to the spectrum of unreacted OA
267 particles (i.e. before deliberate ozone exposure). Our data are all for conditions where only a
268 small fraction of gas-phase ozone ($< 10\%$) is consumed by reactive uptake. Data from three
269 different ozone concentrations are mapped onto a consistent ozone exposure ($P_{\text{O}_3}t$) scale; the
270 individual time series are provided in the supplementary information (Figure S2).



271



272

273 Figure 4: (a) Relative intensity of m/z 281.2486 ion corresponding to $[\text{OA} - \text{H}]^-$ as a function of ozone
 274 exposure ($P_{\text{O}_3}t$). On this scale, the data map well onto a single exponential best fit curve, suggesting that
 275 OA loss scales linearly with $[\text{O}_3 \text{ (g)}]$. (b) Time series for 8ppm ozone for ions assigned to primary C_9
 276 products of oleic acid ozonolysis: nonanoic acid (NA), 9-oxononanoic acid (9-ON), and azaleic acid
 277 (AA). The ion intensities were scaled to their value at 140 s when essentially all of the oleic acid was
 278 depleted, and hence the symbols for NA, 9-ON and AA overlap at this time. The curve represents a
 279 hypothetical first-order production term from oleic acid; this describes NA and AA relatively well at short
 280 times but does not capture the behavior of 9-ON.
 281

282 The consensus from previous particle-phase observations, based on the functional form and
 283 pronounced size dependence of OA loss, is that ozone reacts rapidly once accommodated onto
 284 oleic acid particles [*Morris et al.*, 2002; *Smith et al.*, 2002; *Hearn and Smith*, 2004; *Hearn et al.*,
 285 2005; *Ziemann*, 2005]. The exponential fit to all of our data in Figure 4(a) is consistent with the
 286 formulation of *Hearn et al.* [2005] for reaction in a surface film (case 3 kinetics):

$$287 \frac{[\text{OA}]}{[\text{OA}]_0} = \exp\left(-\frac{3\delta^2}{r} K_{\text{H},\text{O}_3} k^{\text{II}} P_{\text{O}_3} t\right) \quad (1)$$

288 Where δ is the thickness of the surface film, r is the particle radius, K_{H,O_3} is the Henry's law
 289 coefficient for ozone in oleic acid, k^{II} is the ozonolysis rate constant in the film, P_{O_3} is the ozone
 290 partial pressure and t is the reaction time. Our data from three different ozone concentrations are
 291 well described by a single fit to Equation (1) in Figure 4(a). Consistent with this formulation, our
 292 OA loss rate is a linear function of ozone concentration in the flow tube; we extracted pseudo-
 293 first order loss rates for each concentration from Figure 4(a) which are listed in Table S2.
 294 Previous data have been presented on an ozone exposure scale [*Morris et al.*, 2002; *Hearn and*
 295 *Smith*, 2004], but to our knowledge this linearity in $[\text{O}_3 \text{ (g)}]$ has not been explicitly demonstrated
 296 before. We note that any possible secondary losses of oleic acid from other reactants such as
 297 Criegee intermediates do not perturb pseudo-first order OA losses and are therefore likely of
 298 minor importance.

299 The oleic acid loss measurements also enable us to derive a reactive uptake coefficient for ozone
 300 onto the aerosols. We follow the approach of *Hearn et al.* [2005] for reaction in a surface film
 301 and calculate $\gamma = 5 (\pm 2) \times 10^{-4}$. This is relatively low compared to $\gamma \sim 8 \times 10^{-4}$ recommended by
 302 the review of *Zahardis and Petrucci* [2007], but is within the combined experimental

303 uncertainty. This compares well to a recent determination by *Al-Kindi et al.*, [2016] and lower
 304 values have been reported in other studies [*Dennis-Smith et al.*, 2012].

305 **3.3. Kinetics of product formation**

306 EESI-MS allows us to monitor changes in a variety of products, including complex secondary
 307 species which are difficult to analyse using many alternative approaches. Now that we have
 308 established that the oleic acid loss rate is first order in $[O_3 (g)]$, we present the remaining data as
 309 a function of time rather than ozone exposure for more explicit comparison with PG-AM. We
 310 consider first the primary C_9 products, and Figure 4(b) shows measured time series for nonanoic
 311 acid (NA), 9-oxononanoic acid (9-ON) and azelaic acid (AA) for particles exposed to the lowest
 312 of the three ozone concentrations, 8 ppm. In this case ion intensities are scaled to a nominal final
 313 value when essentially all of the oleic acid had reacted.

314 These products are formed from the initial ozone-alkene reaction, either directly or via CI-
 315 isomerization (Figure 2(a)). If we assume the particle-phase CI lifetime is short, we might
 316 therefore expect the products to all exhibit the same time dependence based on the characteristic
 317 timescale for oleic acid loss $k^1 = 0.050 \text{ s}^{-1}$ from Table S3. The black curve in Figure 4(b)
 318 illustrates a calculated first-order production term alongside the measurements. We ascribe
 319 differences between the species, and deviation from this curve, to non-first order processes,
 320 specifically oligomer formation reactions. The NA and AA data show a very similar time
 321 dependence which is close to the calculated curve over most of the reaction, although some
 322 differences can be seen at 40 s. This suggests that the loss processes for these species are
 323 relatively small. By contrast, the relative concentration of 9-ON deviates from this first-order
 324 behavior. We hypothesize that this is due to a bimolecular sink for 9-ON, such as reaction with
 325 CI:

$$326 \frac{d[9\text{-ON}]}{dt} = k_{OA+O_3}[OA][O_3] - k_c[9\text{-ON}][CI] \quad (2)$$

327 The production term is unchanged from the black curve in Figure 4(b) and will be largest at the
 328 start of the reaction. However, the loss term will increase as 9-ON builds up. On a relative
 329 concentration scale, the net effect of this scenario is to make the product time series approach a
 330 maximum more rapidly, consistent with the observed 9-ON profile. We quantitatively assess the

331 importance of this reaction and other particle-phase processes using an explicit numerical aerosol
332 model in the following section.

333 4. Model simulations of experimental observations

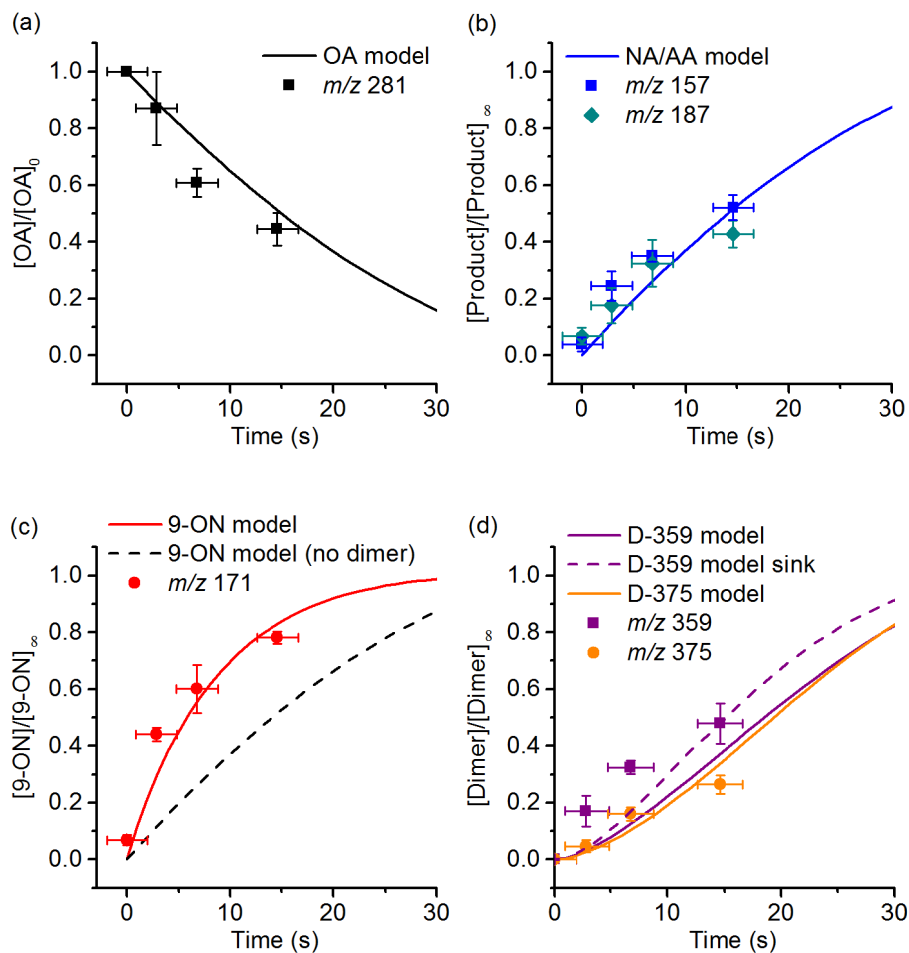
334 4.1. EESI-MS data

335 To better understand the time dependence of our aerosol chemical composition measurements,
336 we introduce a model which explicitly simulates the underlying processes relevant to organic
337 aerosol aging, the Pretty Good Aerosol Model (PG-AM). This framework also allows us to
338 investigate other observations such as the size-dependent reactivity of oleic acid particles
339 [Morris *et al.*, 2002; Smith *et al.*, 2002] and particle volume changes as a consequence of ozone
340 uptake and product evaporation [Dennis-Smith *et al.*, 2012]. Figure 5 shows modelled time
341 series for oleic acid and a range of primary and secondary products alongside the EESI-MS
342 measurements. The oleic acid losses (Figure(a)) are captured well by the model using the
343 literature parameters specified in Table S1. The accommodation coefficient α_{O_3} is a poorly
344 constrained parameter for this system, and $\alpha_{O_3} = 10^{-3}$ was found to give a good fit to the data in
345 Figure 5(a) and for the higher ozone concentrations (Figure S3).

346 The model shows a strong radial gradient in $[O_3(l)]$ during the simulation (Figure S4) which is
347 consistent with the picture of rapid ozone reaction following accommodation to the particle. As a
348 consequence, the modelled oleic acid loss rate exhibits a profound particle size dependence. We
349 characterized the competition between ozone diffusion through the particle and reaction with an
350 oleic acid molecule in terms of a reacto-diffusive length, $l = D_{O_3}/k_{O_3+OA}[OA]$. For $r_{\text{eff}} = 250$ nm
351 used here, we obtained $l < 8$ nm for the early part of the reaction, indicating that the ozone
352 remains confined to the outer few percent of the particle until most of the oleic acid is consumed.
353 This agrees well with an experimental estimate of reacto-diffusive length of 10 nm [Morris *et al.*,
354 2002]. The oleic acid, meanwhile, shows only small gradients due to rapid bulk diffusion, in
355 agreement with the modelling study of Shiraiwa *et al.* [2010] and consistent with particles
356 remaining liquid throughout ozonolysis [Hosny *et al.*, 2016].

357 We also simulated product formation and secondary chemistry occurring in the particles. Since
358 the rates of oligomer formation reactions are not at all known, we proceeded by fixing $k_a = 500$ s⁻¹

359 ¹ based on *Welz et al.* [2012], and varying the oligomerization reaction rates (k_b and k_c) to obtain
 360 the best fit to the MS data. We found that the model was not sensitive to the absolute magnitude
 361 of k_a , provided $k_a \gg k^1$.



362

363

364 Figure 5: Modelled concentrations as a function of time for (a) oleic acid (OA), (b) nonanoic acid (NA)
 365 and azaleic acid (AA), (c) 9-oxononanoic acid (9-ON) and (d) dimer products, dimer-359 and dimer-375.
 366 EESI-MS measurements with 8 ppm ozone are included as discrete points and both model and
 367 experimental results are scaled to aid comparison. The model shows a close fit to the measured OA (a)
 368 and primary product ((b) and (c)) data, and reasonable agreement for the dimer products (d). NA and AA
 369 (b) have the same modelled time dependence owing to the symmetry of the mechanism (Figure 2). The
 370 dashed line in (c) represents a simulation with the dimer chemistry switched off, and the dashed line in (d)
 371 includes a unimolecular sink for D-359 ($k_{\text{sink}} = 0.01 \text{ s}^{-1}$) as a proxy for further dimer reactions.

372

373 Agreement between the modelled and measured concentrations was found for all of the product
 374 species (Figure 5(b)-(d)), given the experimental and parametric uncertainty involved in this
 375 comparison. In particular, the characteristic difference in the 9-ON time series compared to the

376 other primary products noted in Figure 4(b) was reproduced by including the oligomerization
377 reactions described in Figure 2(b).

378 9-oxononanoic acid contains an aldehyde functional group as well as the acid group also present
379 in azaleic acid and nonanoic acid. We therefore found the predominant reaction of 9-ON with
380 Criegee intermediates to be via the aldehyde group (k_c), with a relatively lower rate of CI-acid
381 reaction (k_b) for all three C₉ products. The dashed line in Figure 5(c) shows the simulated 9-ON
382 profile with oligomerization switched off, a demonstrably poorer agreement. The products of CI-
383 aldehyde reactions are secondary ozonides (SOZs), and our results are consistent with evidence
384 from the solution-phase literature that SOZs form in high yields [*Geletneky and Berger, 1998;*
385 *Carey and Sundberg, 2008*]. However, they contrast with the findings of *Mochida et al. [2006]*
386 who reported that the highest dimer yields from oleic acid ozonolysis result from CI-acid
387 reactions.

388 Since the model is not sensitive to the absolute magnitude of k_a , the relative rates k_b/k_a and k_c/k_a
389 determine the fate of the CIs in the particle, specifically the branching between isomerization and
390 oligomerization. We found $k_b/k_a = 0.3 \text{ M}^{-1}$ and $k_c/k_a = 2 \text{ M}^{-1}$ respectively gave good fits to the
391 primary product time series (Figure 5(b) and (c)).

392 Figure(d) shows the modelled dimer concentrations, which show reasonable agreement with the
393 experimental values. We found that the modelled profiles were only weakly sensitive to the
394 relative rates k_b/k_a and k_c/k_a and so we used the primary product time series to constrain these
395 ratios. The simulated D-359 profile is initially too low, possibly as a consequence of missing
396 reactions which consume the dimer. The dashed line in Figure 5(d) shows a model run with a
397 pseudo first order dimer loss included ($k_{\text{sink}} = 0.01 \text{ s}^{-1}$) as a proxy for possible further
398 decomposition or oligomerization reactions. This improves the agreement for D-359 in an
399 analogous manner to 9-ON, but the nature of this removal could not be reliably identified from
400 the observed products.

401 **4.1. Simulation of other experimental data**

402 A number of previous studies have presented measurements amenable to process modelling. We
403 focus on three experimental studies which present explicit time dependent measurements of oleic

404 acid concentration changes [*Hearn and Smith, 2004; Ziemann, 2005; Dennis-Smith et al.,*
 405 2012]. These studies span a range of particle sizes, reaction times and ozone concentrations and
 406 so present a test of the model performance. The studies are summarized in Table 2. In each case,
 407 the model parameters were as used as presented in Table S1, while α_{O_3} was adjusted to obtain a
 408 good fit to the oleic acid loss measurements.

Study	Particle radius (nm)	[O ₃] (ppm)	Model parameters	Experimental
This work	~ 250	8-22	Base case (Table S1)	Aerosol ensemble from nebulizer (ethanol solution); flow tube; EESI-MS
<i>Ziemann</i> [2005]	~ 200	2.8	$\alpha_{O_3} = 2 \times 10^{-3}$	Aerosol ensemble by homogeneous nucleation; smog chamber; TDPBMS
<i>Hearn and Smith</i> [2004]	~ 400	100	$\alpha_{O_3} = 1.5 \times 10^{-3}$	Aerosol ensemble from nebulizer (pure OA); flow tube; Aerosol CIMS
<i>Dennis-Smith et al.</i> , [2012]	4580 (core-shell*)	6	$\alpha_{O_3} = 5 \times 10^{-4}$	OA coagulation with single NaCl core*; optical tweezers; Raman and Mie scattering

409 Table 2: Summary of experimental studies of oleic acid aerosol ozonolysis containing explicit time series
 410 for oleic acid loss. The measurements were compared to model simulations under the same conditions and
 411 the best agreement was obtained by adjusting the accommodation coefficient for ozone, α_{O_3} , as a proxy
 412 for experimental and parametric uncertainty. (*) The particles consisted of a liquid oleic acid droplet of
 413 the specified total radius, containing an unreactive sodium chloride inclusion of approximately 2 micron
 414 radius (spherically equivalent size).

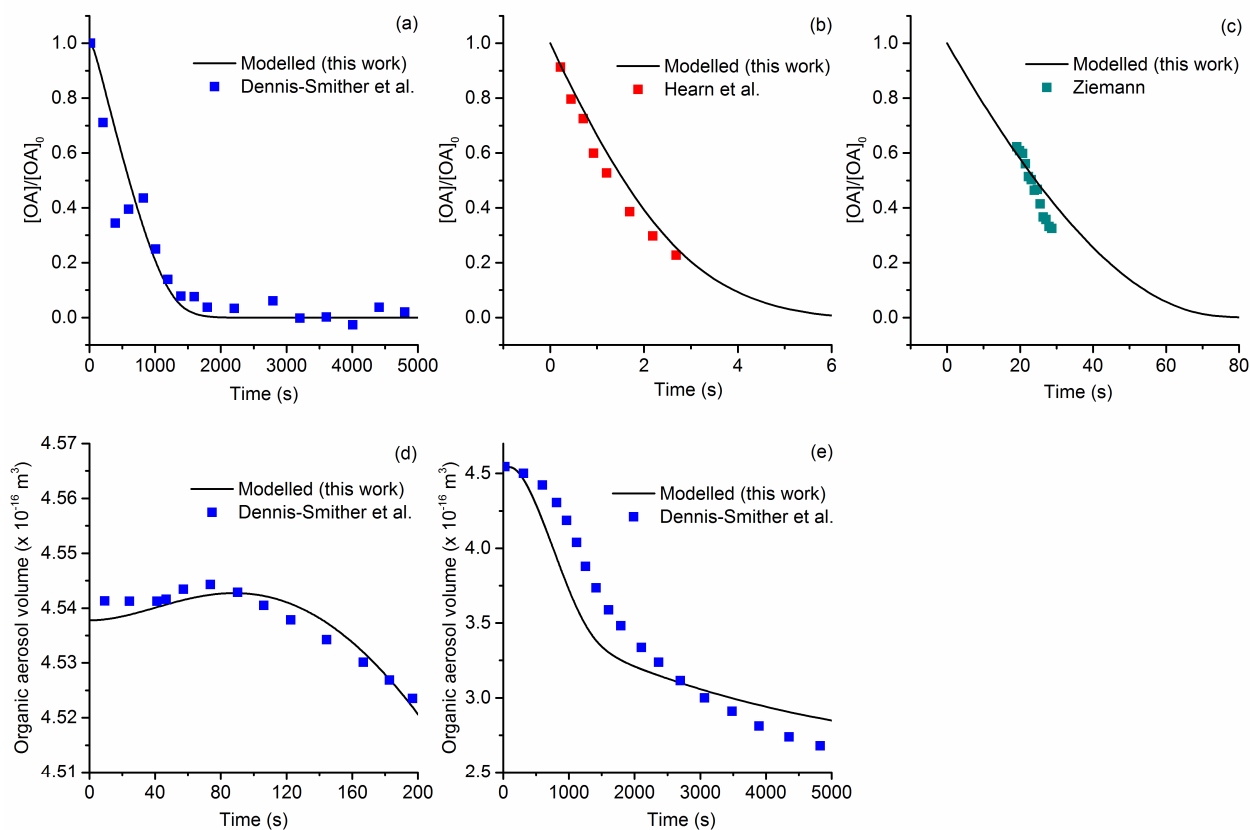
415

416 In general, the model does well in reproducing these observations over a range of particle sizes
417 (~200-5000 nm) and oxidation timescales (seconds-10s of minutes) using the same diffusion and
418 reaction parameters as before. Figure 6(a) shows oleic acid loss data for the *Dennis-Smith et al.*
419 *et al.*, [2012] study, for a single micron-sized particle. We were able to reproduce other studies to a
420 similarly high degree of agreement, and the time series for *Hearn and Smith* [2004] and *Ziemann*
421 [2005] are presented in Figures 6(b) and (c) respectively. We feel that close model agreement
422 with a range of measurements helps to rationalize previous observations and provide a more
423 coherent picture of the ozonolysis of oleic acid particles with respect to relevant physico-
424 chemical parameters (Table S1).

425 The modified α_{O_3} values can be seen as a reflection of the variation of measured loss rates: For
426 instance, *Dennis-Smith et al.* [2012] note that their oleic acid loss is slower relative to the sub-
427 micron particle studies. Nevertheless, α_{O_3} was only varied by $\pm 50\%$ to obtain good agreement
428 across this range of measurements, consistent with the experimental uncertainty on such
429 determinations which is usually high. The more significant reduction in α_{O_3} for the case of
430 *Dennis-Smith et al.* [2012] may also be the result of the different experimental approaches. Our
431 composition measurements involve sampling a steady state ozone-exposed aerosol ensemble
432 from a flow tube, while the static chamber set-up used in the single particle study may have
433 required a non-negligible gas phase equilibration time, leading to lower and uncertain ozone
434 concentrations early in the reaction. We also note the different methods of aerosol preparation: in
435 our case, we prepared the aerosol from an OA solution using a nebuliser, while in *Dennis-*
436 *Smith et al.* [2012] the aerosol was prepared from the coagulation of homogeneously nucleated
437 OA particles with a sodium chloride “core” particle in the optical trap. Given the combined
438 experimental uncertainty, and possible systematic differences in particle properties, we consider
439 the agreement is very encouraging.

440 In addition to oleic acid loss from particles, we investigated the particle evaporation behavior
441 presented in *Dennis-Smith et al.* [2012] using PG-AM. The same chemical scheme as Figure 2
442 was used again here, and gas-particle partitioning coefficients for oleic acid and each of the C₉
443 products were calculated according to their saturation vapor pressures (Table S1). Dimer
444 products were assumed to be non-volatile.

445 The model captures the observed size changes over both short and long time scales. The small
 446 initial increase in volume (Figure 6(d)), corresponding to only a few nanometers in radius, is
 447 explained in the model by the formation of volatile products, particularly nonanal, whose initial
 448 evaporation rate from the particle is lower than its production rate. The consequence is an initial
 449 build-up of particle-phase nonanal followed by evaporation on longer time scales (Figure 6(e)).



450

451 Figure 6: Model simulations compared with observations of oleic acid loss for (a) *Dennis-Smith et al.*,
 452 [2012], (b) *Hearn et al.*, [2004] and (c) *Ziemann* [2005]. We also simulate the single particle volume
 453 change of *Dennis-Smith et al.*, (d) at the start of ozonolysis and (e) over the experiment timescale. The
 454 model parameters were as for the base case (Table S1) with changes according to the experiment-specific
 455 parameters in Table 2. For the simulation in (b), precision and accuracy checks were turned off from
 456 Mathematica's NDSolve routine to allow the model to execute. The experimental data in (c) were
 457 obtained directly from P. Ziemann since the Figure presented in *Ziemann* [2005] contains a small error.
 458 These data were offset in time to coincide with the simulated curve and account for the mixing period in
 459 the chamber experiment.

460

461 The relatively slow initial evaporation of nonanal, despite its high vapor pressure, would be
 462 reconciled by a small accommodation coefficient for nonanal and hence slow transfer out of the
 463 particle. $\alpha_{\text{org}} = 10^{-5}$ was used in the model, which also leads to the gradual evaporation of

464 nonanoic acid and 9-oxononanoic acid on long timescales after the OA was consumed. This is
465 consistent with the hypothesis of *Dennis-Smith et al.*, [2012] for their continuing particle
466 volume loss. Slow evaporation behaviour may also be a consequence of changes in diffusion
467 within the particle which are not considered in the model. *Hosny et al.*, [2016] observed that the
468 viscosity of oleic acid aerosol increased during ozonolysis, while *Lee et al.*, [2012] hypothesized
469 that an amorphous “crust” formed on the surface of arachidonic acid during ozonolysis, which
470 like oleic acid is an unsaturated, hydrophobic acid. *Dennis-Smith et al.*, [2012] observed a
471 longtime increase in the apparent refractive index retrieved from the evaporating droplet,
472 assuming the particle was homogeneous, even after the size had reached a steady value. This was
473 considered to indicate the possible slow relaxation in a concentration gradient within the particle
474 or a restructuring in particle morphology.

475 The magnitude of the modelled and measured evaporative losses are comparable over the course
476 of the reaction (Figure 6(e)). However, there is an overprediction of evaporation at short times
477 and slight underprediction at longer times. The model chemical scheme favors formation of
478 nonanal and azaleic acid from the initial cycloaddition reaction; adjusting this branching ratio
479 closer to 1:1 to favor more (semivolatile) nonanoic acid and 9-oxononanoic acid production
480 would reconcile these differences.

481 We revisit the ozonolysis mechanism to interpret some of the kinetic parameters derived from
482 this model analysis. Decomposition of the unstable primary ozonide (Figure 2(a)) forms the
483 initial functional groups (CI and aldehyde) in close proximity and oriented towards each other,
484 which may promote transient intermolecular interaction between the products. Furthermore,
485 previous studies have noted that the surrounding fatty acid medium is likely to be ordered into a
486 rod-like arrangement of molecules [*Iwahashi et al.*, 2000] owing to the propensity for oleic acid
487 to form hydrogen-bonded acid pairs. These geometric constraints may lead to formation of a
488 “caged” CI-aldehyde complex.

489 In such a scenario, the CI encounters a high effective aldehyde concentration immediately,
490 whereas other bimolecular reactions require CI reorientation and diffusion. This is a plausible
491 explanation for the much larger 9-ON sink (k_c) than for the other C₉ products (k_b). However, CI

492 escape must occur to some extent, to explain the latter hydroperoxide products and also
493 secondary ozonides produced by cross reactions from two ozonolysis events, such as m/z 359.

494 The slow evaporation of nonanal, represented in the model by a small mass accommodation
495 coefficient, could also be a consequence of restricted escape from such a “caged” geometry.
496 Using a larger value for accommodation ($\alpha_{\text{nonanal}} \sim 0.1$) would require a lifetime for the complex
497 on the order of 10s of seconds to explain the evaporation data. This would appear to be long for a
498 transient complex, possibly suggesting a role for decomposition of initial products (such as
499 oligomers) to yield nonanal, as hinted at by the dimer “sink” reaction discussed in Figure 5(d).
500 Ultimately, however, the available data do not permit us to distinguish between these hypotheses.

501

502 **4.2. Comparison with other modelling studies**

503 Utilizing a detailed model can provide insight into aerosol processes as demonstrated in the
504 sections above. However, it is important to recognize that the model requires appropriate and
505 physically realistic constraints, specifically in terms of the input parameters used to represent
506 reaction, diffusion and interfacial transport. Our preference is to fix as many of the parameters as
507 possible based on literature values, either from experiment or theory. Fortunately, for the oleic
508 acid-ozone system, a relatively large quantity of relevant parametric data are available and
509 consequently few parameters were optimized by comparison with experimental data. We find
510 that the parameters reported in Table S1 can adequately describe experimental observations
511 within combined experimental and parametric uncertainties.

512 Similar “fixed parameter” case studies have also proven successful in detailed modelling by
513 *Shiraiwa et al.* [2010] and *Houle et al.*, [2015] for heterogeneous aging of organic aerosols. An
514 alternative approach which samples more of the model parameter space by globally optimising
515 parameter sets with respect to experimental aerosol measurements has been reported recently
516 [*Berkemeier et al.*, 2016]. This approach may be particularly useful if important parameters are
517 not readily available from the literature for the system of interest. *Berkemeier et al.*, [2016] point
518 out that large experimental data sets are required to adequately constrain degrees of freedom in
519 the model, but we note that even for a relatively well studied system such as the reactive uptake

520 of ozone to oleic acid particles, appreciable differences in key parameters such as $k_{\text{OA}+\text{O}_3}$ can
521 arise ($k_{\text{PG-AM}}/k_{\text{Hosny}} \sim 1500$) [Hosny *et al.*, 2016]. Both approaches may help to assess and
522 constrain relevant physico-chemical aerosol parameters in future.

523

524 Conclusions

525 The combination of measurement and modelling presented in this study represents an important
526 step forward in the detailed understanding of organic aerosol processes, especially for systems
527 such as the ozonolysis of oleic acid aerosol where competition between transport and reaction
528 determines the timescale for atmospheric processing.

529 The ability of EESI-MS to make aerosol kinetics measurements on a molecular level has been
530 demonstrated for the first time using the ozonolysis of oleic acid aerosol as a model system.
531 Useful quantitative information could be derived from the relative intensities of $[\text{M} - \text{H}]^-$
532 reactant and product ions in the EESI mass spectra.

533 A process-level model was used to interpret these measurements and complementary
534 observations from previous studies. Differences in the measured appearance rates of ozonolysis
535 products were used to constrain the relative rates of secondary reactions in the particles. We
536 concluded that the lifetime of Criegee intermediates in the particle was short with respect to
537 isomerization, but that a significant sink for CIs may involve secondary ozonide formation
538 through reaction with the aldehyde group of 9-ON. The reaction between oleic acid and ozone
539 was found to occur in a near-surface layer, in good agreement with experimental studies.

540 Model performance was further assessed by comparison to other studies with large differences in
541 timescales, ozone concentrations and particle sizes. Chemical and evaporative changes were both
542 reproduced well. Significantly, the chemical insight provided by the new product measurements
543 was used to construct a model chemical mechanism able to successfully explain independent
544 measurements of the evolving particle size. Comparing to multiple experimental observables
545 both improves confidence in the model performance and strengthens the conclusions of
546 experimental work.

547 The difficulty of interrogating the kinetics of reactive intermediates in particles was
548 demonstrated in this study. This represents an ongoing challenge for the organic aerosol
549 community. Including a mechanism for CI reactions in the model allowed relative rates (e.g.
550 k_c/k_a) to be assessed and represents a useful starting point. However, since the rate determining
551 step for product formation was the initial ozone-alkene cycloaddition, absolute rates of CI
552 reactions could not be determined. In addition, there are inherent limits to process modelling
553 based on the unavailability or uncertainty of relevant physical parameters for the system under
554 study. Nevertheless, our methodology provides insight into the kinetic regimes and chemical
555 changes associated with organic aerosol aging, and these issues will be addressed in future
556 studies.

557

558 Acknowledgements

559 This work was supported by the European Research Council (ERC starting grant 279405 and the
560 ERC Atmospheric Chemistry Climate Interactions (ACCI) project). We thank the Reviewers for
561 insightful and constructive feedback on the manuscript. Data may be obtained from the
562 University of Cambridge Data Repository at <https://doi.org/10.17863/CAM.7996> (Note: This
563 placeholder link will be activated as required).

564

565 References

- 566 Al-Kindi, S., F. D. Pope, D. C. Beddows, W. J. Bloss, and R. M. Harrison (2016), Size dependent chemical ageing
567 of oleic acid aerosol under dry and humidified conditions, *Atmos. Chem. Phys. Discuss.*, 1–44,
568 doi:10.5194/acp-2016-230.
- 569 Barsanti, K. C., and J. F. Pankow (2005), Thermodynamics of the formation of atmospheric organic particulate
570 matter by accretion reactions - 2. Dialdehydes, methylglyoxal, and diketones, *Atmos. Environ.*, 39(35), 6597–
571 6607, doi:10.1016/j.atmosenv.2005.07.056.
- 572 Barsanti, K. C., and J. F. Pankow (2006), Thermodynamics of the formation of atmospheric organic particulate
573 matter by accretion reactions-Part 3: Carboxylic and dicarboxylic acids, *Atmos. Environ.*, 40(34), 6676–6686,
574 doi:10.1016/j.atmosenv.2006.03.013.
- 575 Berkemeier, T., A. J. Huisman, M. Ammann, M. Shiraiwa, and T. Koop (2013), and heterogeneous reactions in
576 atmospheric aerosols and clouds : a general classification scheme, , 6663–6686, doi:10.5194/acp-13-6663-
577 2013.
- 578 Berkemeier, T., S. S. Steimer, U. K. Krieger, T. Peter, U. Pöschl, M. Ammann, and M. Shiraiwa (2016), Ozone
579 uptake on glassy, semi-solid and liquid organic matter and the role of reactive oxygen intermediates in
580 atmospheric aerosol chemistry, *Phys. Chem. Chem. Phys.*, 18(18), 12662–12674, doi:10.1039/C6CP00634E.

- 581 Boucher, O. et al. (2013), Clouds and Aerosols, in *Climate Change 2013: The Physical Science Basis. Contribution*
582 *of Working Group I to the Fifth Assessment Report of the Intergovernmental Panel on Climate Change*, edited
583 by T. F. Stocker, D. Qin, G.-K. Plattner, M. Tignor, S. K. Allen, J. Boschung, A. Nauels, Y. Xia, V. Bex, and
584 P. M. Midgley.
- 585 Carey, F. A., and R. J. Sundberg (2008), *Advanced Organic Chemistry*, Fifth Edit., Springer.
- 586 Dennis-Smith, B. J., R. E. H. Miles, and J. P. Reid (2012), Oxidative aging of mixed oleic acid/sodium chloride
587 aerosol particles, *J. Geophys. Res. Atmos.*, *117*(20), 1–13, doi:10.1029/2012JD018163.
- 588 Gallimore, P. J., and M. Kalberer (2013), Characterizing an extractive electrospray ionization (EESI) source for the
589 online mass spectrometry analysis of organic aerosols, *Environ. Sci. Technol.*, *47*(13), 7324–31,
590 doi:10.1021/es305199h.
- 591 Geletnek, C., and S. Berger (1998), The Mechanism of Ozonolysis Revisited by 17O-NMR Spectroscopy,
592 *European J. Org. Chem.*, (8), 1625–1627, doi:10.1002/(SICI)1099-0690(199808)1998:8<1625::AID-
593 EJOC1625>3.0.CO;2-L.
- 594 Griffiths, P. T., C. L. Badger, R. A. Cox, M. Folkers, H. H. Henk, and T. F. Mentel (2009), Reactive uptake of
595 N₂O₅ by aerosols containing dicarboxylic acids. Effect of particle phase, composition, and nitrate content, *J.*
596 *Phys. Chem. A*, *113*(17), 5082–5090, doi:10.1021/jp8096814.
- 597 Hearn, J. D., and G. D. Smith (2004), Kinetics and Product Studies for Ozonolysis Reactions of Organic Particles
598 Using Aerosol CIMS †, *J. Phys. Chem. A*, *108*(45), 10019–10029, doi:10.1021/jp0404145.
- 599 Hearn, J. D., A. J. Lovett, and G. D. Smith (2005), Ozonolysis of oleic acid particles: evidence for a surface reaction
600 and secondary reactions involving Criegee intermediates., *Phys. Chem. Chem. Phys.*, *7*(3), 501–11.
- 601 Hosny, N. A. et al. (2016), Direct imaging of changes in aerosol particle viscosity upon hydration and chemical
602 aging, *Chem. Sci.*, *7*, 1357–1367, doi:10.1039/C5SC02959G.
- 603 Houle, F. A., W. D. Hinsberg, and K. R. Wilson (2015), Oxidation of a model alkane aerosol by OH radical: the
604 emergent nature of reactive uptake., *Phys. Chem. Chem. Phys.*, *17*(6), 4412–4423, doi:10.1039/c4cp05093b.
- 605 Iwahashi, M., Y. Kasahara, H. Matsuzawa, K. Yagi, K. Nomura, H. Terauchi, Y. Ozaki, and M. Suzuki (2000), Self-
606 Diffusion, Dynamical Molecular Conformation, and Liquid Structures of n-Saturated and Unsaturated Fatty
607 Acids, *J Phys Chem B*, *104*, 6186–6194.
- 608 Katrib, Y., S. T. Martin, H.-M. Hung, Y. Rudich, H. Zhang, J. G. Slowik, P. Davidovits, J. T. Jayne, and D. R.
609 Worsnop (2004), Products and Mechanisms of Ozone Reactions with Oleic Acid for Aerosol Particles Having
610 Core-Shell Morphologies, *J. Phys. Chem. A*, *108*, 6686–6695.
- 611 Keyser, L. F. (1984), High-Pressure Flow Kinetics. A Study of the OH + HCl Reaction from 2 to 100 torr, *J. Phys.*
612 *Chem.*, *88*(20), 4750–4758.
- 613 Kroll, J. H., and J. H. Seinfeld (2008), Chemistry of secondary organic aerosol: Formation and evolution of low-
614 volatility organics in the atmosphere, *Atmos. Environ.*, *42*(16), 3593–3624,
615 doi:10.1016/j.atmosenv.2008.01.003.
- 616 Lee, J. W. L., V. Carrascón, P. J. Gallimore, S. J. Fuller, A. Björkegren, D. R. Spring, F. D. Pope, and M. Kalberer
617 (2012), The effect of humidity on the ozonolysis of unsaturated compounds in aerosol particles, *Phys. Chem.*
618 *Chem. Phys.*, *14*(22), 8023–31, doi:10.1039/c2cp24094g.
- 619 Liggio, J., and S. M. Li (2006), Reactive uptake of pinonaldehyde on acidic aerosols, *J. Geophys. Res. Atmos.*,
620 *111*(24), 1–12, doi:10.1029/2005JD006978.
- 621 McNeill, V. F., J. L. Woo, D. D. Kim, A. N. Schwier, N. J. Wannell, A. J. Sumner, and J. M. Barakat (2012),
622 Aqueous-phase secondary organic aerosol and organosulfate formation in atmospheric aerosols: A modeling
623 study, *Environ. Sci. Technol.*, *46*, 8075–8081, doi:10.1021/es3002986.
- 624 Mochida, M., K. Yasuyuki, K. Kawamura, Y. Nojiri, and K. Suzuki (2002), Fatty acids in the marine atmosphere:
625 Factors governing their concentrations and evaluation of organic films on sea-salt particles, *J. Geophys. Res.*,
626 *107*(D17), 4325, doi:10.1029/2001JD001278.
- 627 Mochida, M., Y. Katrib, J. T. Jayne, D. R. Worsnop, and S. T. Martin (2006), The relative importance of competing
628 pathways for the formation of high-molecular-weight peroxides in the ozonolysis of organic aerosol particles,
629 *Atmos. Chem. Phys. Discuss.*, *6*(4), 7137–7176, doi:10.5194/acpd-6-7137-2006.
- 630 Morris, J. W., P. Davidovits, J. T. Jayne, J. L. Jimenez, Q. Shi, C. E. Kolb, and D. R. Worsnop (2002), Kinetics of
631 submicron oleic acid aerosols with ozone: A novel aerosol mass spectrometric technique, *J. Geophys. Res.*,
632 *107*(9), 3–6.
- 632 Murphy, D. M., D. J. Cziczo, K. D. Froyd, P. K. Hudson, B. M. Matthew, A. M. Middlebrook, R. E. Peltier, A.
633 Sullivan, D. S. Thomson, and R. J. Weber (2006), Single-particle mass spectrometry of tropospheric aerosol
634 particles, *J. Geophys. Res.*, *111*, D23S32, doi:10.1029/2006JD007340.
- 635 Noziere, B. et al. (2015), The Molecular Identification of Organic Compounds in the Atmosphere: State of the Art
and Challenges, *Chem. Rev.*, *115*(10), 3919–3983, doi:10.1021/cr5003485.

- 637 Pope, C. A., M. Ezzati, and D. W. Dockery (2009), Fine-particulate air pollution and life expectancy in the United
638 States, *N. Engl. J. Med.*, *360*(4), 376–86, doi:10.1056/NEJMsa0805646.
- 639 Reynolds, J. C., D. J. Last, M. McGillen, A. Nijs, A. B. Horn, C. Percival, L. J. Carpenter, and A. C. Lewis (2006),
640 Structural analysis of oligomeric molecules formed from the reaction products of oleic acid ozonolysis,
641 *Environ. Sci. Technol.*, *40*(21), 6674–6681.
- 642 Robinson, A. L., N. M. Donahue, M. K. Shrivastava, E. A. Weitkamp, A. M. Sage, A. P. Grieshop, T. E. Lane, J. R.
643 Pierce, and S. N. Pandis (2007), Rethinking Organic Aerosols: Semivolatile Emissions and Photochemical
644 Aging, *Science* (80-.), *315*, 1259–1262.
- 645 Rogge, W. F., L. M. Hildemann, M. A. Mazurek, G. R. Cass, and B. R. T. Simonelt (1993), Sources of Fine Organic
646 Aerosol. 2. Noncatalyst and Catalyst-Equipped Automobiles and Heavy-Duty Diesel Trucks, *Environ. Sci.*
647 *Technol.*, *27*, 636–651.
- 648 Rudich, Y., N. M. Donahue, and T. F. Mentel (2007), Aging of organic aerosol: bridging the gap between laboratory
649 and field studies., *Annu. Rev. Phys. Chem.*, *58*, 321–352, doi:10.1146/annurev.physchem.58.032806.104432.
- 650 Shiraiwa, M., C. Pfrang, and U. Pöschl (2010), Kinetic multi-layer model of aerosol surface and bulk chemistry
651 (KM-SUB): the influence of interfacial transport and bulk diffusion on the oxidation of oleic acid, *Atmos.*
652 *Chem. Phys.*, *10*(1), 281–326, doi:DOI 10.5194/acp-10-3673-2010.
- 653 Smith, G. D., E. Woods, C. L. DeForest, T. Baer, and R. E. Miller (2002), Reactive Uptake of Ozone by Oleic Acid
654 Aerosol Particles: Application of Single-Particle Mass Spectrometry to Heterogeneous Reaction Kinetics, *J.*
655 *Phys. Chem. A*, *106*(35), 8085–8095, doi:10.1021/jp020527t.
- 656 Stewart, D. J., P. T. Griffiths, and R. A. Cox (2004), Reactive uptake coefficients for heterogeneous reaction of
657 N₂O₅ with submicron aerosols of NaCl and natural sea salt, , (2), 1381–1388, doi:10.5194/acpd-4-569-2004.
- 658 Vereecken, L., H. Harder, and A. Novelli (2014), The reactions of Criegee intermediates with alkenes, ozone, and
659 carbonyl oxides., *Phys. Chem. Chem. Phys.*, *16*(9), 4039–49, doi:10.1039/c3cp54514h.
- 660 Vesna, O., M. Sax, M. Kalberer, A. Gaschen, and M. Ammann (2009), Product study of oleic acid ozonolysis as
661 function of humidity, *Atmos. Environ.*, *43*(24), 3662–3669, doi:10.1016/j.atmosenv.2009.04.047.
- 662 Wang, G., K. Kawamura, S. Lee, K. Ho, and J. Cao (2006), Molecular, Seasonal, and Spatial Distributions of
663 Organic Aerosols from Fourteen Chinese Cities, *Environ. Sci. Technol.*, *40*(15), 4619–4625,
664 doi:10.1021/es060291x.
- 665 Wang, M., L. Yao, J. Zheng, X. Wang, J. Chen, X. Yang, D. R. Worsnop, N. M. Donahue, and L. Wang (2016),
666 Reactions of Atmospheric Particulate Stabilized Criegee Intermediates Lead to High-Molecular-Weight
667 Aerosol Components, *Environ. Sci. Technol.*, acs.est.6b02114, doi:10.1021/acs.est.6b02114.
- 668 Welz, O., J. D. Savee, D. L. Osborn, S. S. Vasu, C. J. Percival, D. E. Shallcross, and C. A. Taatjes (2012), Direct
669 Kinetic Measurements of Criegee Intermediate (CH₂OO) Formed by Reaction of CH₂I with O₂, *Science* (80-
670), *335*, 204–207, doi:10.1126/science.1213229.
- 671 Zahardis, J., and G. A. Petrucci (2007), The oleic acid-ozone heterogeneous reaction system: products, kinetics,
672 secondary chemistry, and atmospheric implications of a model system – a review, *Atmos. Chem. Phys.*, *7*(5),
673 1237–1274, doi:10.5194/acp-7-1237-2007.
- 674 Zahardis, J., B. W. LaFranchi, and G. A. Petrucci (2005), Photoelectron resonance capture ionization-aerosol mass
675 spectrometry of the ozonolysis products of oleic acid particles: Direct measure of higher molecular weight
676 oxygenates, *J. Geophys. Res. D Atmos.*, *110*(8), 1–10, doi:10.1029/2004JD005336.
- 677 Zhao, R., E. L. Mungall, A. K. Y. Lee, D. Aljawhary, and J. P. D. Abbatt (2014), Aqueous-phase photooxidation of
678 levoglucosan – a mechanistic study using Aerosol Time of Flight Chemical Ionization Mass Spectrometry
679 (Aerosol-ToF-CIMS), *Atmos. Chem. Phys. Discuss.*, *14*(7), 8819–8850, doi:10.5194/acpd-14-8819-2014.
- 680 Ziemann, P. J. (2005), Aerosol products, mechanisms, and kinetics of heterogeneous reactions of ozone with oleic
681 acid in pure and mixed particles, *Faraday Discuss.*, *130*, 469–490, doi:10.1039/b417502f.
- 682 Ziemann, P. J., and R. Atkinson (2012), Kinetics, products, and mechanisms of secondary organic aerosol
683 formation, *Chem. Soc. Rev.*, *41*(19), 6582–605, doi:10.1039/c2cs35122f.
- 684